Contents list available at **IJND**

International Journal of Nano Dimension

Journal homepage: *www.IJND.ir*

Effect of Al$_2$O$_3$-water nanofluid on heat transfer and pressure drop in a three-dimensional microchannel

G. A. Sheikhzadeh
M. Ebrahim Qomi
N. Hajialigol[*]
A. Fattahi

Department of Mechanical Engineering, University of Kashan, Kashan, Iran.

ABSTRACT

The fluid flow and heat transfer in a three-dimensional microchannel filled with Al$_2$O$_3$- water nanofluid is numerically investigated. The hybrid scheme is used to discretize the convection terms and SIMPLER algorithm is adopted to couple the velocity and pressure field in the momentum equations. The thermal and flow fields were analyzed using different volume fractions of nanoparticles and different Reynolds numbers. The temperature fields, the average Nusselt number on the bottom surface, the thermal resistance and the pressure drop were obtained from the simulations. Results indicated enhanced performance with the usage of nanofluids, and slight penalty in pressure drop. The increase in Reynolds number caused increase in the heat transfer rate as well as pressure drop and decrease in the thermal resistance.

Keywords: *Nanofluid; Microchannel; Convection heat transfer; Pressure drop.*

* Corresponding author:
Najmeh Hajialigol
Department of Mechanical
Engineering, University of
Kashan, Kashan, Iran.
Tel +98 3615912443
Fax +98 3615912475
Email najmeh.hajialigol@gmail.com

INTRODUCTION

Over two decades ago, microchannels emerged as a potential solution for dissipating thermal energy from densely packed integrated circuitry. Researches indicated that high heat fluxes could be dissipated by a working fluid passing through microchannels that offer an increased surface area to volume ratio. In the early 1980s, Tuckerman and Pease [1] reported that a microchannel heat sink could dissipate as much as 790 W/cm^2 with 71 K mean fluid temperature rise. Because of high heat flux produced by compact integrated circuitries, there is a growing necessity for novel researches into design, performance, and application of microchannel.

Li and Peterson [2] proposed three-dimensional semi-normalized numerical method to explore the optimal geometry of the parallel microchannel heat sinks and demonstrated that on a silicon wafer with a typical thickness of 450 μm, the configurations first used by Tuckerman and Pease [1] and by Kawano et al. [3], were quite close to the optimized values predicted by the numerical model. Nevertheless, the ultimate optimal geometry was not achieved due to the constraint of the wafer thickness of 450 μm. Tullius et al. [4] comprehensively reviewed the cooling performance of microchannels with various designs and different fluids. Air, water and fluoro-chemicals are the most common fluids used in their microchannels. The heat transfer performance of these fluids is limited, however, due to their transport properties and/or low thermal conductivity.

To enhance the thermal conductivity of working liquids and accordingly further improving in performance of the liquid-cooled microchannel heat sinks, the application of nanofluids in microchannels has gained much attention in recent years. Lee and Choi [5] have found that the nanofluid in the microchannel heat exchanger dramatically enhances cooling rate compared with the conventional water cooled and liquid-nitrogen-cooled microchannel heat exchangers. In a numerical hydrodynamic and thermal study of laminar fully developed flows of copper– and diamond–water nanofluids [6], the cooling performance of the microchannel heat sink was found significantly improved as reflected by the marked reduction in the thermal resistance as well as the temperature difference between the heated microchannel wall and the nanofluids. Raisi et al. [7] numerically studied the forced convection of a laminar nanofluid in a microchannel in both slip and no-slip conditions. They argued that making use of nanofluids enhances the heat transfer performance of the microchannel. Aminossadati et al. [8] studied effects of magnetic field on nanofluid forced convection in a partially heated microchannel. Their results showed that the microchannel heat is more transferred at higher values of the Reynolds numbers and magnetic field.

In this paper, the fluid flow and heat transfer performance of a water– Al_2O_3 nanofluid in the three- dimensional microchannel is studied. The hybrid scheme is used to discretize the convection terms and SIMPLER algorithm is adopted to couple the velocity and pressure field in the momentum equations.

EXPERIMENTAL

Figure 1 shows a schematic diagram of the three- dimensional microchannel considered in this study according to work of Mlcak et al. [9]. It is assumed that the microchannel is manufactured by Silicon. Dimensions of the schematic geometry are shown in Table 1. Microchannel surface aspect ratios (Ar) are w_c/h_c=0.1and hydraulic diameter (D_h) of that is 86.6 μm. The bottom surface with dimensions of w×l is heated with a constant and uniform heat flux of q´´=90 kw/m^2. The other microchannel walls are thermally insulated. The temperature of the water– Al_2O_3 nanofluid at the microchannel inlet is T_c=298 K
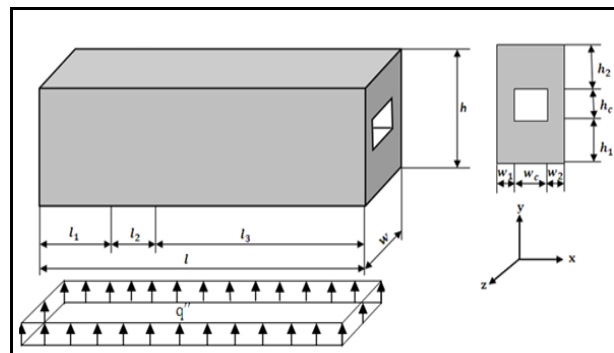

Fig. 1. A schematic geometry of the physical model

Table 1. Dimensions of the microchannel (μm)

h	h_c	l	l_1	l_2	w	w_c
900	476	10000	3478	4348	100	47.6

Governing equations and numerical procedure

The non-dimensional governing equations of continuity, momentum and energy are presented as follows:

$$\frac{\partial U}{\partial X} + \frac{\partial V}{\partial Y} + \frac{\partial W}{\partial Z} = 0 \tag{1}$$

$$U\frac{\partial U}{\partial X} + V\frac{\partial U}{\partial Y} + W\frac{\partial U}{\partial Z} = -\frac{\partial P}{\partial X} + \frac{1}{Re \times \vartheta_f \times \rho_{nf,0}}\left[\frac{\partial}{\partial X}\left(\mu_{nf}\frac{\partial U}{\partial X}\right) + \frac{\partial}{\partial Y}\left(\mu_{nf}\frac{\partial U}{\partial Y}\right) + \frac{\partial}{\partial Z}\left(\mu_{nf}\frac{\partial U}{\partial Z}\right)\right] \tag{2}$$

$$U\frac{\partial V}{\partial X} + V\frac{\partial V}{\partial Y} + W\frac{\partial V}{\partial Z} = -\frac{\partial P}{\partial Y} + \frac{1}{Re \times \vartheta_f \times \rho_{nf,0}}\left[\frac{\partial}{\partial X}\left(\mu_{nf}\frac{\partial V}{\partial X}\right) + \frac{\partial}{\partial Y}\left(\mu_{nf}\frac{\partial V}{\partial Y}\right) + \frac{\partial}{\partial Z}\left(\mu_{nf}\frac{\partial V}{\partial Z}\right)\right] + \frac{(\rho\beta)_{nf}}{\beta_f\rho_{nf,0}}Ri\theta \tag{3}$$

$$U\frac{\partial W}{\partial X} + V\frac{\partial W}{\partial Y} + W\frac{\partial W}{\partial Z} = -\frac{\partial P}{\partial Z} + \frac{1}{Re \times \vartheta_f \times \rho_{nf,0}}\left[\frac{\partial}{\partial X}\left(\mu_{nf}\frac{\partial W}{\partial X}\right) + \frac{\partial}{\partial Y}\left(\mu_{nf}\frac{\partial W}{\partial Y}\right) + \frac{\partial}{\partial Z}\left(\mu_{nf}\frac{\partial W}{\partial Z}\right)\right] \tag{4}$$

$$U\frac{\partial \theta}{\partial X} + V\frac{\partial \theta}{\partial Y} + W\frac{\partial \theta}{\partial Z} = \frac{1}{Re \times Pr \times \alpha_f \times (\rho c_p)_{nf}}\left[\frac{\partial}{\partial X}\left(K_{nf}\frac{\partial \theta}{\partial X}\right) + \frac{\partial}{\partial Y}\left(K_{nf}\frac{\partial \theta}{\partial Y}\right) + \frac{\partial}{\partial Z}\left(K_{nf}\frac{\partial \theta}{\partial Z}\right)\right] \tag{5}$$

$$\left[\frac{\partial}{\partial X}\left(K_s\frac{\partial \theta}{\partial X}\right) + \frac{\partial}{\partial Y}\left(K_s\frac{\partial \theta}{\partial Y}\right) + \frac{\partial}{\partial Z}\left(K_s\frac{\partial \theta}{\partial Z}\right)\right] = 0 \tag{6}$$

In the above equations, the following non-dimensional parameters are used:

$$X = \frac{x}{D_h} \qquad Y = \frac{y}{D_h} \qquad Z = \frac{z}{D_h} \qquad U = \frac{u}{u_c}$$

$$V = \frac{v}{u_c} \qquad W = \frac{w}{u_c} \qquad P = \frac{p}{\rho_{nf}u_c^2} \qquad \theta = \frac{T - T_C}{\Delta T} \tag{7}$$

$$\Delta T = \frac{q''D_h}{k_f} \qquad Re = \frac{u_c D_h}{\vartheta_f} \qquad Pr = \frac{\vartheta_f}{\alpha_f}$$

Where, U, V and W are the velocity components, P the pressure, θ the temperature, ρ the density, g the gravitational acceleration, ν the dynamic viscosity and β the coefficient of thermal expansion, The properties of the nanofluid can be defined based on the properties of water and Alumina:

$$\rho_{nf} = (1 - x_c)\rho_f + x_c\rho_{np} \tag{8}$$

$$(\rho c_p)_{nf} = (1 - x_c)(\rho c_p)_f + x_c(\rho c_p)_{np} \tag{9}$$

$$\alpha_{nf} = \frac{k_{nf}}{(\rho c_p)_{nf}} \tag{10}$$

Here, x_c is the volume fraction of nanoparticles, and the subscripts f, nf and np stand for the base fluid, nanofluid and nanoparticles, respectively. The effective thermal conductivity of the nanofluid calculated by the Chon et al. model [10] is:

$$\frac{k_{nf}}{k_f} = 1 + 64.7 x_c^{0.4076}\left(\frac{d_f}{d_p}\right)^{0.3690}\left(\frac{k_p}{k_f}\right)^{0.7476} Pr_T^{0.9955} Re^{1.2321} \tag{11}$$

Here Pr_T and Re are defined by:

$$Pr_T = \frac{\mu_f}{\rho_f\alpha_f} \tag{12}$$

$$Re = \frac{\rho_f k_b T}{3\pi\mu_f l_f} \tag{13}$$

k_b=1.3807×10-23 J/K, is the Boltzmann constant and l_f =0.17 nm is the mean path of fluid particles [10]. The viscosity of the nanoparticle (Al_2O_3) is:

$$\mu_{nf} = \exp\left(\begin{array}{c} 3.003 - 0.04203T - 0.5445x_c \\ +.00002553T^2 + 0.0524x_c{}^2 - 1.622x_c{}^{-1} \end{array}\right) \times 10^{-3}$$

(14)

The temperature in equation (14) is expressed by Celsius. Nusselt number on the bottom surface is calculated as follows:

$$Nu_s = \frac{\frac{\Delta Tk_f}{D_h}D_h}{k_f(\theta_{w,m}(X) \times \Delta T - \theta_m(X) \times \Delta T)} = \frac{1}{(\theta_{w,m}(X) - \theta_m(X))}$$

(15)

Where:

$$\theta_{w,m}(X) \times \Delta T = \frac{\Delta T}{p_s}\int \theta_w(Y,Z)dS \qquad \textbf{(16)}$$

$$\theta_m(X) \times \Delta T = \frac{\Delta T}{U_m A_c}\int_{L_1}^{L_2}\int_{H_1}^{H_2} U(Y,Z)\theta(Y,Z)dYdZ \qquad \textbf{(17)}$$

$$U_m = \frac{\int_{L_1}^{L_2}\int_{H_1}^{H_2} U(X,Y)dYdZ}{\int_{L_1}^{L_2}\int_{H_1}^{H_2} dYdZ} \qquad \textbf{(18)}$$

Here, P_s and S are channel perimeter and surface along channel perimeter, respectively. The subscript w stands for microchannel wall. Finally, the average Nusselt number on the bottom surface is determined from:

$$Nu_{avg} = \frac{\int_0^l \frac{dX}{(\theta_{w,m}(X) - \theta_m(X))}}{\int_0^l dX} \qquad \textbf{(19)}$$

The inlet and outlet thermal resistance value, R, as defined by equations (20) and (21) was used to monitor the behavior of the temperature field.

$$R_{inlet} = \frac{\theta_{wmax,inlet}\,\Delta T}{\frac{\Delta Tk_f}{D_h}} = \frac{D_h\theta_{wmax,inlet}}{k_f} \qquad \textbf{(20)}$$

$$R_{outlet} = \frac{\theta_{wmax,outlet}\,\Delta T}{\frac{\Delta Tk_f}{D_h}} = \frac{D_h\theta_{wmax,outlet}}{k_f} \qquad \textbf{(21)}$$

The governing equations associated with the boundary conditions are solved numerically using the control-volume based finite volume method. The hybrid-scheme, which is a combination of the central difference scheme and the upwind scheme, is used to discretize the convection terms. In order to couple the velocity and pressure field in the momentum equations, the well-known SIMPLER-algorithm was adopted. Grid independency of the solution is investigated for the standard case. The solution of the fully coupled discretized equations is obtained iteratively using TDMA method. In this study, various grid sizes are tested to guarantee a grid independent solution for x_c=0.02. It is found that a grid size of 141×71×31 ensures a grid independent solution.

RESULTS AND DISCUSSION

The accuracy of results is verified by comparison the results with the available data published by Aminossadati et al. [8] as depicted in Figures 2 and 3. In these figures, red and black lines are for the present and reference results, respectively. In addition, Table 2 compares the average Nusselt number obtained by the present study with those of Lo *et al*. [11] in a three-dimensional cavity. The current results are in good agreement with references results.
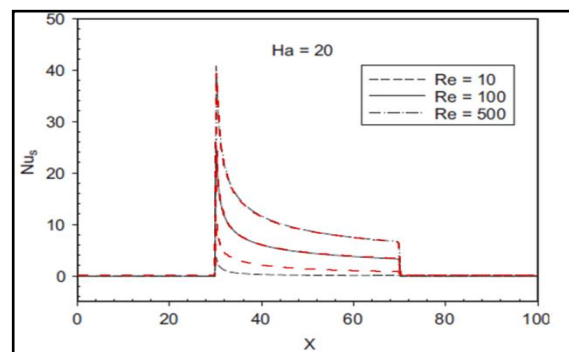

Fig. 2. Variation of local Nusselt number along the channel length

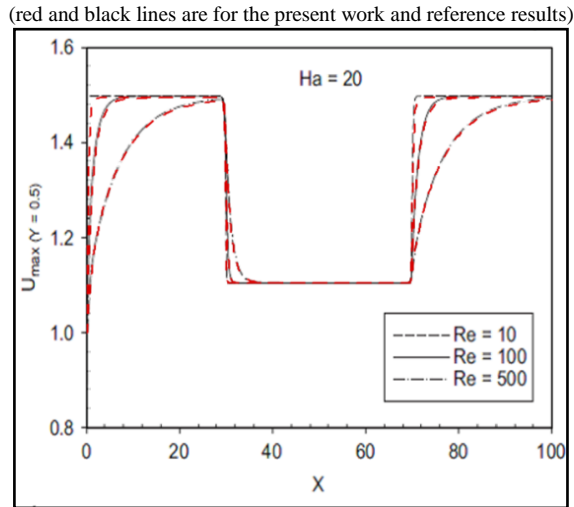(red and black lines are for the present work and reference results)

Fig. 3. Variation of horizontal velocity along the centerline
of the channel(red and black lines are for
the present work and reference results)

Table 2. Comparison between average Nusselt number: of the
present work and data of Lo et al. [11].

Ra	10^3	10^4	10^5	10^6
Present work	1.0715	2.0623	4.03853	8.5316
Lo *et al.* [11]	1.0884	2.0537	4.03329	8.5766

The numerical analysis is carried out to find the influence of nanofluid use on mixed convection in the three-dimensional microchannel. The study is executed for $0 \leq x_c \leq 0.06$, $50 \leq Re \leq 400$, Ar=0.1 and Pr = 6.2. The temperature fields, average Nusselt number on the bottom surface, the thermal resistance and the pressure drop are surveyed. Temperature distributions for various volume fractions of nanoparticles at Re=200 in X=30, 55, 70 and 100 are illustrated in Figure 4. This figure shows that for all volume fractions of nanoparticles, the temperature in both the nanofluid and the microchannel wall solid rise with increasing distance from the channel entrance. It is also evident that the high temperature regions in the microchannel walls decrease as volume fractions of nanoparticles increase.
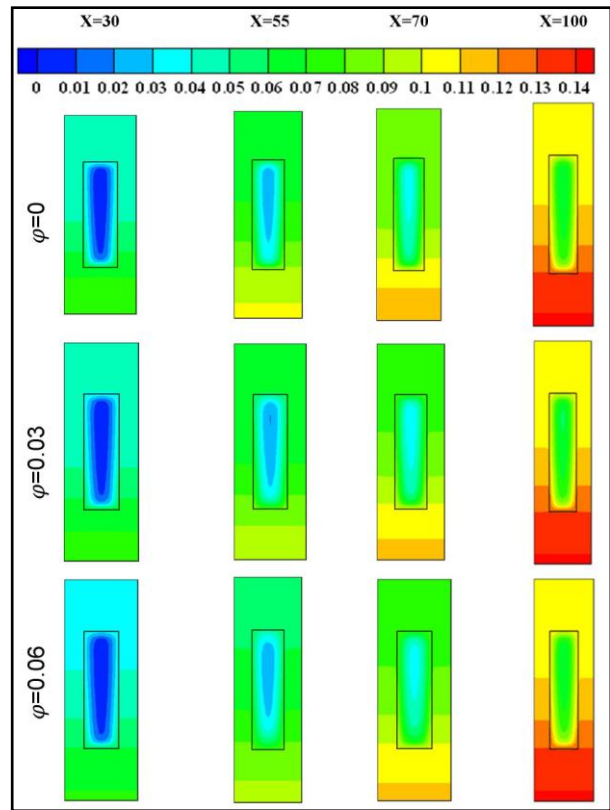

Fig. 4. Isotherms for in the cross-section of the channel with various
volume fractions of nanoparticles (Re=200).

The influences of the Reynolds number and various volume fractions of the nanoparticles on the average Nusselt number on the bottom surface are graphically presented in Figure 5. It is evident that average Nusselt number increases with increase in the volume fraction of the nanoparticles. This behavior is evident from the fact that the heat transfer can be enhanced due to the increases in both the stagnant thermal conductivity of the nanofluid and the thermal dispersion conductivity when the dispersed particles concentration increases. In addition, the difference of enhancement between different Reynolds numbers presumably occurred because the mechanism of heat transfer enhancement for the nanofluids was different for the different flow conditions. At higher Reynolds number, more particles are taking part in heat transport and there is higher surface area of particles interacting with the base fluid, thereby enhancing the heat transfer process. The Nusselt number of higher Reynolds numbers, presented more enhancement by increasing x_c compared with low Reynolds numbers. Generally

the Nusselt number of nanofluid is higher than that of the base fluid (water) as the presence of nanoparticles results in an increase of thermal conductivity. Nusselt number enhances with increasing Reynolds number due to the intensification of the nanofluid mixing fluctuation.
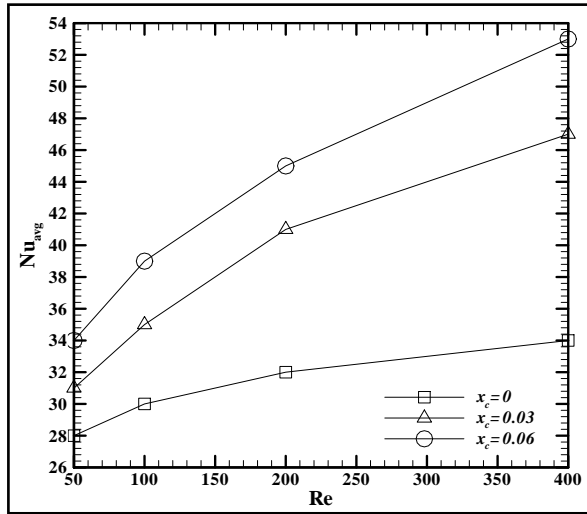

Fig. 5. Average Nusselt number on the bottom surface versus Reynolds number for various volume fractions of nanoparticles.

Values of increment in the Nusselt number of nanofluid compared to results of the base fluid are shown in Table 3 for the different particle volume fraction and minimum and maximum Reynolds numbers (Re=50 and 400). It is observed that by increasing the x_c, Nusselt number increases. All nanofluids have a higher Nusselt number compared to the base fluid. It can see using nanofluids at high Reynolds numbers compared with low Reynolds numbers, have higher average Nusselt number. The importance of this result unfolds by considering the results of pressure drop. The increase of nanofluid concentration has the following consequences: the increases of thermal conductivity and collision of nanoparticles which are favorite factors for heat transfer enhancement and an increase of fluid viscosity which diminishes the fluid movement and thus heat transfer rate. In concentration range studied, the effect of the increase in thermal conductivity and the collision of nanoparticles are more prominent than the increase of the fluid viscosity.

Table 3. The percentage of increment of average Nusselt number compared to the base fluid at low and high Reynolds numbers

x_c	0.01	0.02	0.03	0.04	0.05	0.06
Re=50	3	5	11	17	24	32
Re=400	14	27	38	40	43	45

Figure 6 depicts the values of the pressure drop versus Reynolds number for various volume fractions of nanoparticles. It is observed that by increasing the Reynolds number or x_c, the pressure drop increases. Nanofluid indicated higher pressure drop compare with the base fluid. Obviously, friction factor increases with increasing in concentration of nanoparticles due to the rise of working fluid viscosity. The pressure drop get more enhances at the higher Reynolds number by increasing x_c.
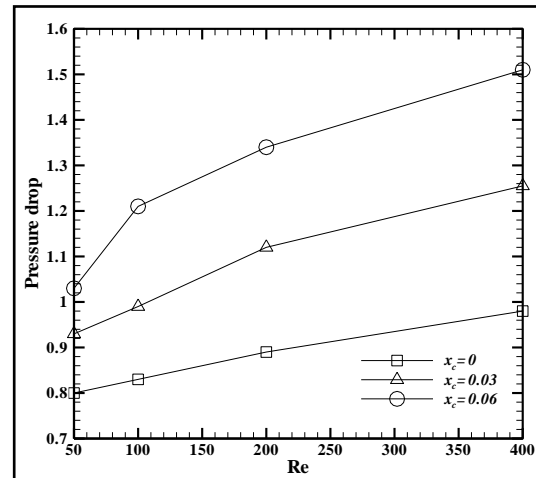

Fig. 6. Pressure drop versus Reynolds number for various volume fractions of nanoparticles.

Figure 7 shows values for thermal resistance at both the inlet and outlet of microchannel for all considered Reynolds numbers and various volume fractions of nanoparticles. The values of thermal resistance have an inverse correlation with heat transfer. Local convection coefficients are larger at the channel inlet than at the channel outlet because of entry effects. When

more thermal energy is transferred to the base fluid or nanofluid near the channel entrance, the surface temperature near the channel entrance will decrease and the resistance will be low. If less energy is transferred to the base fluid or nanofluid near the channel entrance, the convection coefficient will be low, which will increase the surface temperature in this region as well as the resistance. As outlined in Figure 7, rising Reynolds number causes to decrease in thermal resistance at both the channel outlet and inlet. For high Reynolds numbers, the surface temperatures became very close to the liquid inlet temperatures resulting in a low thermal resistance. From Figure 7, it is clear that increasing in the investigated range of Reynolds numbers, the thermal resistance is reduced when nanofluid is applied as coolant. This enhancement in heat transfer indicates that nanofluids could be a promising replacement for pure water in microchannel where there is need to more efficient heat transfer.
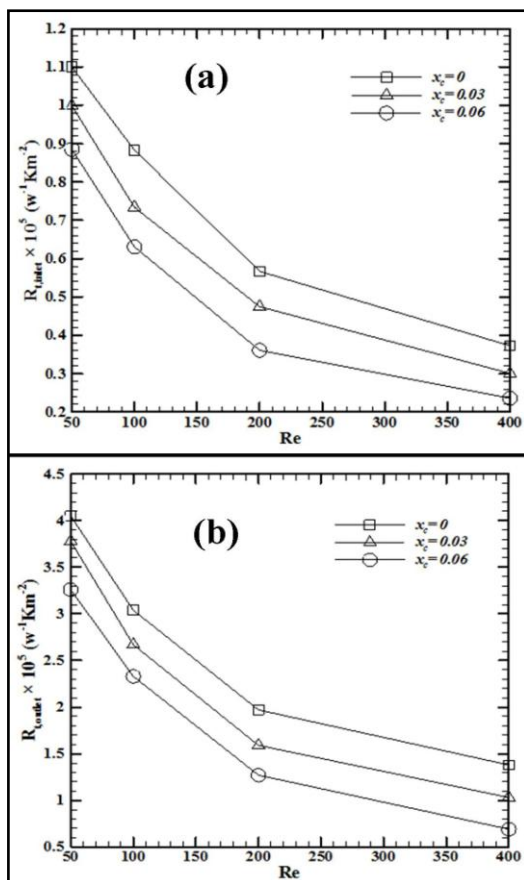

Fig. 7. Thermal resistance value versus Reynolds number for various volume fractions of nanoparticles: (a) At the inlet of microchannel, (b) At the outlet of microchannel.

CONCLUSIONS

A numerical model was utilized to simulate a three dimensional fluid flow and heat transfer in a three-dimensional microchannel filled with Al_2O_3- water nanofluid. Based on the present numerical study, the following results are obtained:

• For all values of volume fractions of nanoparticles, the temperature in fluid, nanofluid and microchannel wall increase versus increasing distance from the channel entrance.

• Addition of nanoparticles increased average Nusselt number, which indicated higher heat transfer into the fluids. Thus nanofluids could be a promising replacement for pure water in microchannel where there is need to more efficient heat transfer

• The increase in Reynolds number caused increase in the heat transfer rate as well as pressure drop and decrease in the thermal resistance.

• Using nanofluids compared to the base fluid causes increase in the pressure drop.

• Using nanofluids at high Reynolds numbers compared with low Reynolds numbershave higher average Nusselt number.

REFERENCES

[1] Tuckerman B.D.and PeaseR.F.W., (1981), High-performance heat sinking for VLSI. IEEE Electr. Device Lett. EDL, 2: 136-147.

[2] LiJ., PetersonG.P., (2006),Geometric optimization of a micro heat sink with liquid flow, IEEE Trans. *Compon. Packag. Technol*. 29 (1): 145–154

[3] KawanoK., MinakamiK., IwasakiH., IshizukaM., (1998), Development of micro channels heat exchanging, in: R.A. Nelson Jr., L.W. Swanson, M.V.A. Bianchi, C. Camci (Eds.), Application of Heat Transfer in Equipment, Systems, and Education, HTD-Vol. 361-3/PID-Vol. 3, *ASME, New York*, , 173–180.

[4] TulliusJ.F., VajtaiR., BayazitogluY., (2011),A review of cooling in microchannels, *Heat Transfer Engineering* 32 (7–8): 527–541.

[5] LeeS., ChoiS.U.S., (1996), Applications of metallic nanoparticle suspensions in advanced cooling system, in: Y Kwon, D.C. Davis, H.H.

Chung (Eds.), Recent Advances in Solid/Structures and Application of Metallic Materials, PVP-vol. 342/MD-vol. 72, *ASME, New York*, , 227–234.

[6] JangS.P., ChoiS.U.S., (2006), Cooling performance of a microchannel heat sink with nanofluids, *Appl. Thermal Eng*, 26: 2457-2469.

[7] RaisiA., GhasemiB. and AminossadatiS.M., (2011), A numerical study on the forced convection of laminar nanofluid in a microchannel with both slip and no-slip conditions, Numerical Heat Transfer; *Part A: Applications*, 59 (2): 114-123.

[8] AminossadatiS.M., Raisi A.and GhasemiB., (2011), Effects of magnetic field on nanofluid forced convection in a partially heated microchannel, *Int. J. Non-Linear Mechanics*, 46: 1373-1384.

[9] MlcakJustin D., AnandN.K., RightleyMichael J., (2008), Three-dimensional laminar flow and heat transfer in a parallel array of microchannels etched on a substrate, *Heat and Mass Transfer,* 51: 5128-5137.

[10] SheikhzadehG.A., Ebrahim QomiM., HajialigolN., Fattahi.A., (2012), Numerical study of mixed convection flows in a lid-driven enclosure filled with nanofluid using variable properties, *Results in Physics*, 2: 5-13.

[11] Lo, D.C.,YoungD.L., MurugesanK., TsaiC.C., GouM.H., (2007), Velocity– vorticity formulation for 3D natural convection in an inclined cavity by DQ method. *Heat and Mass Transfer,* 50: 479-484.